

**KERNFORSCHUNGSZENTRUM  
KARLSRUHE**

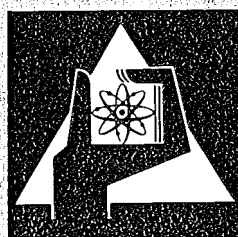
April 1974

KFK 2021

Institut für Angewandte Kernphysik

**Experimental and Theoretical Aspects of  
High Resolution Neutron Spectroscopy**

S. Cierjacks



**GESELLSCHAFT  
FÜR  
KERNFORSCHUNG M.B.H.**

**KARLSRUHE**

Als Manuskript vervielfältigt

Für diesen Bericht behalten wir uns alle Rechte vor

GESELLSCHAFT FÜR KERNFORSCHUNG M. B. H.  
KARLSRUHE

KERNFORSCHUNGSZENTRUM KARLSRUHE

April 1974

KFK 2021

Institut für Angewandte Kernphysik

Experimental and Theoretical Aspects of High Resolution Neutron Spectroscopy

S. Cierjacks

Gesellschaft für Kernforschung m.b.H., Karlsruhe

Lectures given at the II. International School on Neutron Physics, Alushta [Crimea], USSR,  
April 2-19, 1974



## Abstract:

Present experimental conditions for high resolution neutron spectroscopy are discussed on the basis of recent developments in neutron spectrometers using a continuous energy spectrum source. Particular consideration is given to the isochronous cyclotron time-of-flight spectrometer. As an example of this type of facility, the fast neutron spectrometer at the Karlsruhe cyclotron is briefly described. Present specifications of the time-of-flight apparatus are given. To demonstrate its capability for high resolution neutron investigations a few examples of recently obtained results are given. Some theoretical aspects of high resolution neutron spectroscopy are considered in some detail. A new method is discussed which allows an unambiguous assignment of resonance spins and parities by combining results from both high resolution total and a few angle elastic scattering experiments. The implications of this method on the determination of accurate resonance parameters are examined. The appearance of intermediate structure phenomena in fast neutron excitation functions is demonstrated. Its possible interpretation in terms of doorway structure is discussed.

## Zusammenfassung

Die derzeitigen experimentellen Möglichkeiten der hochauflösenden Neutronenspektroskopie werden in diesem Bericht auf der Basis der neueren Entwicklungen leistungsstarker Flugzeitspektrometer diskutiert. Besonderes Gewicht wird auf die Darstellung des Isochronzyklotron-Neutronenspektrometers gelegt. Als ein Beispiel für diesen Spektrometertyp wird das große Flugzeitspektrometer am Karlsruher Zyklotron beschrieben. Dessen Spezifikationen werden angegeben. Um die Leistungsfähigkeit dieser Anlage zu demonstrieren, werden einige charakteristische Ergebnisse von kürzlich durchgeführten hochaufgelösten Messungen gezeigt.

Weiterhin werden einige ausgewählte theoretische Aspekte der Neutronenspektroskopie mit schnellen Neutronen aufgezeigt. Die Grundzüge einer erweiterten Methode zur Identifizierung der Spins und Paritäten von engbenachbarten Zwischenkernresonanzen, welche auf der kombinierten Auswertung totaler sowie differentiell elastischer Querschnitte basiert, werden beschrieben. Der Anwendungsbereich dieser Methode wird geprüft. Derzeit vorliegende experimentelle Hinweise auf die Existenz von intermediären Strukturen in den Anregungsfunktionen von Kernreaktionen mit schnellen Neutronen werden diskutiert. Die Möglichkeit der Interpretation solcher Strukturen auf der Basis des Doorway-Modells wird untersucht.

# EXPERIMENTAL AND THEORETICAL ASPECTS OF HIGH RESOLUTION NEUTRON SPECTROSCOPY

S. Cierjacks

Institut für Angewandte Kernphysik  
Kernforschungszentrum Karlsruhe  
F.R. Germany

Abstract: Present experimental conditions for high resolution neutron spectroscopy are discussed on the basis of recent developments in neutron spectrometers using a continuous energy spectrum source. Particular consideration is given to the isochronous cyclotron time-of-flight spectrometer. As an example of this type of facility, the fast neutron spectrometer at the Karlsruhe cyclotron is briefly described. Present specifications of the time-of-flight apparatus are given. To demonstrate its capability for high resolution neutron investigations a few examples of recently obtained results are given.

Some theoretical aspects of high resolution neutron spectroscopy are considered in some detail. A new method is discussed which allows an unambiguous assignment of neutron resonance spins and parities by combining results from both high-resolution total and a-few angle elastic scattering experiments. The implications of this method on the determination of accurate resonance parameters are examined. The appearance of intermediate structure phenomena in fast neutron excitation function is demonstrated. Its possible interpretation in terms of doorway structure is discussed.

## I. Introduction

The test of modern microscopic theories of nuclear reactions often requires a detailed knowledge of the underlying resonance structure. In particular, accurate resonance parameters

including spin and parity assignments are needed to study systematics of level spacing, level widths and strengths functions and their J and l dependence. Even in this kind of simple study a major difficulty is soon encountered. The rapid decrease of the resolution power of velocity spectrometers with increasing energy results in an increasing number of unresolved resonances, mainly due to higher partial waves. Another type of investigation which suffered severely from the lack of high resolution spectrometers is the study of intermediate structure phenomena. Although there are many experiments, which show strong evidence for the existence of phenomenological intermediate structure, it has not been possible to conclusively identify, with some exceptions<sup>1]</sup>, its nature. In the event that such structure is due to the existence of doorway states, it is necessary that the intermediate resonance in the average cross sections be formed by fine structure resonances all having the same spin and parity. Investigations of this type require very high resolution experiments, since fine structure resonances are typically in the order of  $\sim 1$  keV or below. This figure is typical for medium weight nuclei and neutron energies of up to a few MeV, where most of the evidence for the existence of intermediate structure was observed.

On the basis of these introductory remarks the lecture will be divided into two parts. In the first part recent developments in high resolution neutron spectrometers will be briefly reviewed. Particular consideration will be given to fast neutron spectrometers which are used with isochronous cyclotrons. In the second part a few selected theoretical aspects will be discussed. Major concern will be devoted to spin and parity assignments by means of the  $\alpha$ -few angle scattering method. The application of this method to systematic studies of level spacings, level width and strength functions and their l and J dependence is demonstrated. Finally the usefulness of the combined interpretation of total and partial neutron interactions for the identification of intermediate structure phenomena in terms of doorway states will be outlined.

## II. Experimental Aspects

### A. General

It is well known that level spacings of compound nucleus levels vary systematically with mass number. The level spacings are about 1 MeV for light nuclei, several keV for medium

weight nuclei and less than 1 eV for heavy nuclei. Furthermore, level spacings near magic mass numbers are relatively large compared to their neighbours. Neutron resonance spectroscopy, therefore, covers a wide energy region ranging from electron volts to several MeV. The only technique which has been proven successful for studying this entire energy range is the time-of-flight method. Here, in particular, the pulsed accelerators providing a continuous neutron spectrum are currently the most powerful tools.

To judge the overall quality of a neutron time-of-flight spectrometer, primarily two properties are of importance, i.e. the energy resolution and the neutron intensity which are both closely related.

The effective energy difference  $\Delta E$ , which is distinguishable with a neutron time-of-flight spectrometer, can easily be derived from the non-relativistic energy velocity relation:

$$\Delta E = 2 \frac{\Delta t}{t} \cdot E$$

where  $\Delta t$  is the total time uncertainty produced by the spectrometer and  $t$  is the time needed for the neutron to traverse a flight path of a given length  $L$ .

A more convenient quantity than the energy resolution for our purpose is the logarithmic energy resolution

$$\frac{\Delta E}{E} \sim \frac{\Delta t}{L} \cdot E^{1/2},$$

because it is proportional to a purely instrumental quantity  $\frac{\Delta t}{L}$  and an energy dependent term  $E^{1/2}$ . This relation allows one to derive two consequences.

1. For high energy investigations, high spectrometer resolutions are required.
2. The highest resolving power can be obtained with accelerators having extremely short pulse widths and high average neutron intensities.

The latter condition is due to the fact that the neutron intensity decreases with the quadrat of the flight path length  $L$ . This characterization indicates already that the isochronous cyc-

lotron, with its short pulse lengths of a few nsec and its high average intensities, must be ascribed a particular role for high-resolution fast neutron spectroscopy.

## B. Accelerator-Based Neutron Sources

For high resolution neutron spectroscopy there are primarily four types of modern facilities in use. The electron linear accelerator with booster, the high-current electron linear accelerator, the synchrocyclotron and the isochronous cyclotron. In order to compare different accelerators and their usefulness for time-of-flight experiments, several criteria have been proposed in the past by several authors <sup>2]</sup>. In my opinion the best approach is that suggested by E. Rae from Harwell <sup>3]</sup> which we will adopt in the following discussion. As a measure of the quality of a neutron spectrometer he defined for a given effective energy resolution  $\Delta E/E$  the useful flux available at the detector. In calculating the neutron flux in energy interval  $\Delta E$  of effective energy resolution  $\frac{\Delta E}{E}$ , all inherent components of the spectrometer, such as geometry effects, moderator efficiency, limitations by overlap filters at high repetition rates and low energies etc., must be carefully taken into account. Since the available neutron flux at the detector depends strongly on the energy spectrum provided by different accelerators, the effective neutron flux must be considered as a function of neutron energy.

A comparison employing this criterion for the four mentioned types of accelerators is shown in Fig. 1, which was taken from Rae's work. The neutron flux is plotted here over the energy range from 1 eV to 10 MeV for an effective energy resolution of  $\Delta E/E = 8.8 \times 10^{-4}$ . In particular, the diagram shows the specifications for the Harwell linear accelerator with Booster [HB], the Oak Ridge electron Linear accelerator [ORL], the Harwell Synchrocyclotron [HSC] and the Karlsruhe Sector-Focussed Cyclotron [KSFC]. The numbers in brackets behind the heavy printed symbols are the machine pulse length in nsec. The data given above and below each curve are typical pulse repetition rates and the lengths of flight-paths needed to preserve the constant values of  $\Delta E/E$ . Flight path lengths up to 300 m have been assumed where necessary, irregardless of whether the paths actually exists or not. This flexibility is reasonable, since presently existing flight paths do not necessarily represent the optimum capabilities of the accelerators.

Comparing the different time-of-flight facilities it is apparent that the isochronous cyclotron has the highest neutron intensity and is without competition in the energy range from a few hundred keV up to 30 MeV. In the region of overlap with the other accelerators the isochronous cyclotron has introduced a new order of magnitude in neutron intensity. Furthermore this machine is the only operating facility for continuous measurements in the high MeV range. However, it is not very useful to employ this machine at energies below  $\sim 100$  keV. The high neutron intensity and the narrow pulse width of  $\sim 1$  nsec can only be preserved for high pulse frequencies and unmoderated neutron spectra. We see also that all other machines have their specific merits which can be exploited by careful selection of experiments. The Harwell synchrocyclotron gives the best performance between about 10 and a few hundred keV, while ORELA with 16 and 2.5 nsec pulse operation has the most flexible performance for use over a wide energy range, and is superior to the other machines between  $\sim 100$  eV and 10 keV. The Harwell booster has the best specifications in the range below 100 eV.

In the following the lecture will be restricted to the energy region covered by the isochronous cyclotron neutron spectrometer, e.g. to the range above about 100 keV. The range below will be covered in another lecture at this school given by Dr. Harvey from the Oak Ridge National Laboratory<sup>4]</sup>.

### C. The Karlsruhe Fast Neutron Spectrometer

It has been shown that among the existing particle accelerators the isochronous cyclotron provides the best performance data for fast neutron spectrometers. This machine combines both high average beam intensities and narrow pulse widths of a few nsec. For proper use of this accelerator, however, additional equipment is necessary because isochronous cyclotrons run continuously with a microstructure pulse repetition rate of  $\sim 10 - 30$  MHz. This repetition rate is far too high in view of neutron overlap problems. It is obvious that for long flight paths the time interval of 30 - 100 nsec between two microstructure pulses is so short, that slow neutrons from preceding pulses can be overtaken by fast neutrons from the following bursts. A reduction of the recurrence frequency by suppression of most of the microstructure pulses would entail a tremendous sacrifice in intensity. It is, however, possible to reduce the microstructure pulse repetition rate of an isochronous cyclotron while largely preserving the high average beam intensity of such a machine. This condition has been met

with the Karlsruhe concept of a novel 'deflection bunching' system<sup>5]</sup>. This was developed in its specific form for use with our 50 MeV deuteron machine, but is believed to be unique for isochronous cyclotrons. With the particular system the pulse repetition rate can be reduced from 33 MHz to 200 KHz while the average beam intensity is decreased only by a factor of 3.

Principle of the 'Deflection Bunching' System. The reduction of the pulse repetition rate in the Karlsruhe cyclotron is accomplished by two coupled electrostatic deflector assemblies which together form the "deflection-bunching" system. A schematic drawing of the system is shown in Fig. 2.

In normal continuous operation of the Karlsruhe machine three microstructure pulses per revolution period are accelerated from the source, since the cyclotron is operated in the third harmonic mode. This gives rise to an instantaneous beam distribution as indicated in the top view on the left side by the three azimuthal regions between the dotted lines. The deflector, which is located near the center of the machine [system I], is used for a twofold purpose:

- i] to eliminate two out of three microstructure pulses by deflection to a beam stop and
- ii] to form ion packets of 4.5  $\mu$ sec duration, each consisting of  $\sim 50$  microstructure pulses, with a repetition rate of up to 200 KHz.

As a result of this kind of deflection only the portion of the beam indicated by hatching is accelerated beyond the first deflector system.

Both these objectives have been achieved with a suitable combination of a radial and an axial electrostatic deflector. This is illustrated in Fig. 3. In the upper curve of Fig. 3a the normal continuous pulse structure at the position of the inner deflector is shown. If an accurately phased sine wave of the form shown below is applied to the radial deflector, only every third microstructure pulse passes this system, since the voltage then is decreased to zero. The formation of a 4.5  $\mu$ sec ion packet is explained in Fig. 3b. A constant voltage decreasing to zero for 4.5  $\mu$ sec only once during a burst cycle is applied to an axial deflector of system I which operates on the succeeding orbit. This gives rise to the formation of an ion packet as shown in the lower curve. Since this deflection is accomplished after the 3:1 reduction, microstructure intervals in the ion packet are 90 nsec.

The subsequent procedure with the remaining beam is analogous to the treatment of beam deflection for time-of-flight purposes in synchrocyclotrons. A second axial deflector [system II of Fig. 2a] is positioned at the maximum radius of the machine with the plates above and below the median plane. This deflector serves to simultaneously deflect the whole ion packet to a neutron producing target positioned well above the middle plane [compare Fig. 2b]. At the time of deflection the entire packet, which is distributed over approximately 10 cm in radius, must be completely between the plates of the deflection system II. Before striking the target, the ion packet completes almost an additional revolution. By this geometrical arrangement advantage can be taken of the axial betatron oscillation of the cyclotron.

It is evident that the mentioned treatment produces single neutron pulses of the same duration as the microstructure pulses, i.e. of  $\sim 1$  nsec, but increases the intensity in the neutron burst by almost a factor of 50.

Performance of the Neutron Time-of-Flight Spectrometer. A top view of the spectrometer is shown in Fig. 4. Neutrons are produced by bombardment of a thick natural uranium target with 50 MeV deuterons from the internal cyclotron beam. Collimators are positioned in the flight path to define a narrow neutron beam with a solid angle of  $\sim 2 \times 10^{-6}$  sr. The neutrons are detected at the end of an evacuated flight path, the present length of which is 195 m.

A typical unmoderated time-of-flight spectrum is shown in Fig. 5. The broad pronounced maximum peaked near 18 MeV is due to neutrons from deuteron break-up processes. The flat distribution at energies below 6 MeV originates mainly from evaporation and fission processes. It can be seen from this figure that the useful energy range for measurements with unmoderated spectra is between  $\sim 0.3$  and 30 MeV.

In its present stage of development the Karlsruhe spectrometer has the following performance characteristics: pulse widths  $\sim 1$  ns; repetition rate 20 - 200 kHz variable; time average neutron intensity at 200 kHz -  $2 \times 10^{13}$  n/sr  $\cdot$  sec in the forward direction; spectrometer resolution of nominal 0.005 ns/m, corresponding to an energy resolution of 15 eV at 300 keV and 15 keV at 30 MeV; resolving power -  $5 \times 10^{-5}$  at 300 keV.

#### D. Examples of Typical Measurements

Neutron resonance reactions which can occur in the fast neutron region are total neutron interactions, neutron elastic and inelastic scattering, neutron capture, fission processes and [n,x]-reactions. All types of neutron interactions can be investigated with a continuous energy spectrum neutron time-of-flight spectrometer. Particular types of devices for the study of various total and partial cross sections have been described elsewhere <sup>6-9]</sup>.

A few typical results obtained recently with the Karlsruhe time-of-flight spectrometer might demonstrate the present possibilities in high resolution fast neutron spectroscopy. In Fig. 6 the total neutron cross section for a few elements in the mass range 40 - 60 is shown in a double logarithmic plot. It can be seen that a pronounced structure of resolved, but closely spaced resonances, exists for most of these nuclei up to the energy range of a few MeV. Above this range we can observe rather prominent Ericson fluctuations.

The investigation of elastic scattering with a white source requires a more sophisticated method than normally used in monoenergetic measurements. In order to measure elastic scattering in general, a two parameter set-up is necessary, at least if elastic scattering is to be measured above the inelastic threshold. A feasible method in this case is to determine the incident neutron energy by time-of-flight, and to accomplish the separation between elastic and inelastic scattering events by measurement of the pulse-height from a proton recoil detector. A typical result of a high resolution elastic scattering experiment is shown in Fig. 7. Here the differential elastic scattering cross section of calcium is plotted in the energy range from 1.2 - 2.0 MeV separately for three different angles [upper three curves]. From the bottom curve, which shows the corresponding total neutron cross section, it can be seen that elastic scattering measurements can be carried out with a cyclotron spectrometer with quality and resolution equivalent to transmission measurements.

Neutron inelastic scattering proceeds through the emission of associated prompt  $\gamma$ -rays. Investigation of specific  $\gamma$ -lines by means of a Ge[Li]-detector, therefore, provides - in addition to direct neutron counting - a good method to study inelastic processes. A device of this kind, which has been set up at the Karlsruhe cyclotron <sup>9]</sup> is shown in Fig. 8. Since the efficiency also of large Ge[Li]-detectors is rather low, it is of advantage, to employ a ring geometry for the scatterer. The Ge[Li]-detector is set at a backward angle of  $125^\circ$  and

suitably shielded against neutron and gamma-rays coming directly from the source.

Observation of specific  $\gamma$ -lines leads in turn to  $\gamma$ -ray production cross sections. Assuming that the decay-scheme of the residual nucleus and the multipolarity of the transition is known, the  $\gamma$ -ray production cross sections can be related to inelastic scattering cross sections proceeding through specific inelastic channels. Fig. 9 shows a partial result from a high resolution measurement on iron<sup>9]</sup>. Here the cross section for the inelastic scattering to the 846 keV level of <sup>56</sup>Fe is plotted for the energy range from 0.8- 1.5 MeV. Again we can see that the excitation function shows separated but closely spaced resonances, at least near the threshold.

### III. Theoretical Aspects

#### A. Spin and Parity Assignments of Neutron Resonances from A-Few Angle Elastic Scattering

Differential neutron scattering data have extensively been used in the past for the evaluation of neutron scattering parameters. The methods are highly developed for the lighter nuclei in the form of phase shift analysis. But such investigations were limited to this mass range, primarily because of the previous restrictions in energy resolution. But if high energy resolution measurements are also available, the use of phase shift analysis is not very opportune for medium weight nuclei. In the medium mass range a large number of closely spaced resonances [typically several hundred per MeV energy interval] are existent, so that phase shift analysis becomes very elaborous if at all treatable.

As long as only a few partial waves contribute to resonance scattering, the analysis can be considerably simplified by the method of an a-few angle scattering treatment. It is well known that the resonance shapes of compound-nucleus levels are quite sensitive to spin and parity as a function of the scattering angle. The differences are most apparent at those angles where the Legendre polynomials for the different partial waves cross the zero axis, e.g. the interference terms in the cross sections change sign. While this method has already applied previously by Asami et al.<sup>10]</sup> for an isolated resonance at low energy, it was the work of Nebe and Kirouac<sup>11]</sup> from our laboratory, to extend this method for application in the region of closely spaced resonances.

The theoretical basis for their method is provided by the R-matrix formalism of Wigner<sup>12]</sup> and the formulae of Blatt and Biedenharn<sup>13]</sup>. In the frame work of this theory the pure elastic scattering for partition  $\alpha \rightarrow \alpha$  and channel spin  $s \rightarrow s'$  is given by

$$d\sigma(\alpha s, \alpha s') = \frac{\lambda^2}{2s+1} \sum_{L=0}^{\infty} B_L(\alpha s, \alpha s') P_L(\cos \theta) d\Omega \quad [1]$$

where the coefficients  $B_L$  are defined by

$$B_L(\alpha s, \alpha s') = \frac{1}{4} (-)^{s-s'} \sum \bar{Z}(l_1 J_1, l_2 J_2 / sL) \bar{Z}(l'_1 J_1, l'_2 J_2 / sL) \\ \times \text{Re}(\delta_{s s'} \delta_{l_1 l'_1} - U_{\alpha l_1 s, \alpha l'_1 s'}) (\delta_{s s'} \delta_{l_2 l'_2} - U_{\alpha l_2 s, \alpha l'_2 s'})$$

and the  $\bar{Z}$  coefficients are given as

$$\bar{Z}(l_1 J_1 l_2 J_2 / sL) = l_1^{-L} l_2^{L-l_1-l_2} (2l_1+1)^{1/2} (2J_1+1)^{1/2} (2l_2+1)^{1/2} (2J_2+1)^{1/2} \\ \times W(l_1 J_1 l_2 J_2 / sL) (l_1 l_2 00 / L0)$$

where  $W$  is the Racah<sup>14]</sup> coefficient and the first terms contain the phase correction given by Huby<sup>15]</sup>. The sum is over  $J_1 \pi_1 J_2 \pi_2 l_1 l'_1 l_2 l'_2$ . All sums go from 0 to  $\infty$ . In practice, however, only one sum is really infinite, the other are finite because of selection rules associated with the conservation of parity. Since different values of the channel spin are not observed separately, the cross section  $d\sigma[\alpha s, \alpha s']$  must be summed over all exit channel spins and averaged over the entrance channel spins.

The collision matrix  $U$  is related to the R-matrix by simple functions determined in the external region

$$U = \Omega P^{1/2} [1 - R [L - B]]^{-1} [1 - R [L^+ - B]] P^{-1/2} \Omega$$

where  $\Omega, L$  and  $P$  are the diagonal matrices for the hard sphere phase shift, the logarithmic derivative at the channel surface and the penetration factor, which are all defined in terms of the external wave functions. The channel elements  $R_{cc}$  are given by a sum of resonance terms

$$R_{cc}' = \sum_{\lambda} \frac{Y_{\lambda c} Y_{\lambda c}'}{E_{\lambda} - E}$$

where  $E_{\lambda}$  and  $Y_{\lambda c}$  are the level position and the reduced widths. For elastic scattering there is only a single open channel, so that the R-matrix becomes a simple R-function.

With this formalism it is possible to calculate with a computer program resonance shapes for a series of resonances with different spin and parities which provides a set of standard resonance shapes with which the measured resonance forms can be compared.

A typical result of this type for an even-even medium weight nucleus is shown in Fig. 10. Here typical resonance forms are shown for s-, p- and d-wave resonances which reveals certain characteristics at  $54^{\circ}$ ,  $90^{\circ}$  and  $140^{\circ}$ .

- i] The angular dependence of the shape of an s wave is largely prescribed by the  $L = 0$  term of Eq. [1], thus the resonance amplitude is nearly independent of angle. The slight amplitude decrease at  $90^{\circ}$  and the shift of the resonance peak to lower energies at backward angle are explained by s-waves resonance interference with p-wave potential scattering.
- ii] The p-wave resonances are characterized by a shape change resulting from interference between the resonance and s-wave potential scattering. The interference pattern reverses sign at  $90^{\circ}$ . In the forward quadrant, it is destructive below resonance and constructive above. The interference term vanishes at  $90^{\circ}$  and returns for scattering angles larger than  $90^{\circ}$  with a constructive form below resonance and destructive above. For  $J = 1/2$  the resonance amplitude decreases with increasing angle. Resonances with  $J = 3/2$  increase slightly in height between  $90^{\circ}$  and  $140^{\circ}$  due to the  $L = 2$  term in Eq. 1.
- iii] Resonances due to d-wave neutrons are most notably characterized by the sharply increased amplitude at backward angle and the absence of peak position shifts.

In some cases these general features are modified by resonance-resonance interference. But such effect have also been studied by calculation of characteristic resonance behaviours in case of level-level coherence.

A complete set of neutron resonance parameters can be obtained by combination of the results from high resolution transmission experiments and a few angle scattering measurements. While the differential elastic scattering data allow the unambiguous spin and parity assignments, the resonance energies and widths can be derived from an R-matrix multilevel least squares shape fit to the total cross sections.

A typical result of a combined experiment of this type is shown in Fig. 11. This diagram shows part of the data obtained from a measurement on calcium performed in the energy range between 0.5 and 3.0 MeV. In the upper three curves the differential elastic scattering data at  $140^\circ$ ,  $90^\circ$  and  $54^\circ$  are shown. The bottom curve shows the corresponding total cross section in this partial region from 0.5 - 0.75 MeV. The solid line drawn through the total cross section data represents an R-matrix multilevel fit, based on spin and parity assignments derived from the above scattering data.

With the assignments of a large number of resonances we can examine the systematics of level spacings, level widths and strength functions and perhaps the l and J dependence. Such investigations have been carried out at Karlsruhe for some light and medium weight nuclei.

For the double magic nucleus  $^{40}\text{Ca}$  the combined analysis provided resonance parameters for 70 of 90 resonances observed in the energy region from 0.5-1.5 MeV. Such a number might allow the study of level spacings, separately for s-, p- and d-wave neutrons. The level spacings obtained from the analysis are shown in Fig. 12. The three diagrams show the observed spacings for s-, p- and d-wave neutron resonances. In the two lower diagrams the corresponding fractions for both spin values [dotted and dashed lines] are given separately, in addition to the sum [solid line]. These results are in general agreement with a statistical behaviour. All histograms can be reasonably represented by a straight line through the average data.

For comparison of these results with theoretical predictions, we must take into account that the level spacings are quite sensitive to unresolved resonances. A correction due to this fact can be made by relating the observed level width distribution to the Porter Thomas distribution assuming that the observed integral distributions have a certain fraction of  $\overline{\Gamma}_n^0 / \overline{\Gamma}_n^0$ . The results <sup>11]</sup> obtained by such a treatment are shown in Table 1. The experimentally observed level spacings are listed in column 4. The corrected results for the level spacings

of s-, p- and d-wave neutrons are given in the last column.

Although only 20 - 30 resonances were observed for each partial wave, we might compare the obtained results with theoretical predictions such as from the statistical model. A level density formula which is presently often used, is the formula of Gilbert and Cameron <sup>16]</sup>, which allows separation into an energy dependent and a spin dependent part:

$$\rho[U, J] = G[U] \cdot H[J]$$

where  $H[J]$  is given as

$$H[J] = [2J + 1] e^{-\frac{[J + 1/2]^2}{2\sigma^2}}$$

with  $\sigma^2$  the spin cutoff factor and  $H[J]$  including the density of levels of both parities.

From this formula we would expect an increase of the level density from  $J = 1/2$  to  $J = 3/2$  by almost a factor of two. A reordering of the experimental results in Table I shows, however, that the level densities for  $J = 1/2$  and  $J = 3/2$  reveal the opposite behavior, i.e. the number of  $J = 1/2$  levels is almost twice the number of those for  $J = 3/2$ . We don't have a reasonable explanation for this discrepancy yet. It might be argued, that the  $3/2$  resonances of both parities are less enhanced than the  $1/2$  states, because the investigated energy interval is further away from the corresponding giant resonances, so that less strength is divided between more levels and, therefore, they are not observable with our resolution. But it seems rather improbable from widths and resolution considerations that this fact can account for the large discrepancy of about half an order of magnitude. In addition, such behaviour has qualitatively been found also in high-resolution <sup>48</sup>Ti[p,p]-measurements <sup>17]</sup>.

A similar result of this kind was also observed in an investigation of about 130 resonances of <sup>57</sup>Fe in the region from 400 - 850 keV <sup>18]</sup>. The results have not yet been corrected for missed levels and need final verification by the differential elastic scattering results.

Although the number of p  $1/2$ , p  $3/2$  and d  $3/2$  states might be some 30% higher than quoted, due to corrections for missed levels, these data do not show the predicted strong increase of  $J = 3/2$  levels relative to  $J = 1/2$ . In this case it seems also interesting to mention that Soloviev et al. <sup>19]</sup> have some new calculations for level densities of several spin states for odd and even parities which predicts about 5 times more p  $1/2$  than s  $1/2$  levels near neutron binding. From our preliminary results this can hardly be verified.

Another aspect of neutron resonance analysis is the study of strength functions. This quantity, which represents a measure of the strength of the compound nucleus formation cross section, is defined as

$$S_{IJ} = \Gamma_{nIJ}^{1 \text{ eV}} / \bar{D}_{IJ}$$

and is usually reduced to a neutron energy of 1 eV for comparison with other results. From our investigation one is also able to determine values for this quantity. Some typical results obtained from the calcium data are shown in Table 2. The calculated reduced neutron widths  $\Gamma_n^0$  are shown in column 4, neutron strength functions  $S_{IJ}$  are listed in column 5. The most remarkable result is the low p-wave strength function for this nucleus which supports the earlier suggestion that the p-wave minima are anomalous. The present status of knowledge about p-wave strength function systematics is shown in Fig. 13. This diagram shows a selection of most accurate experimental results compared with optical model calculations using the nonlocal spherical potential of Perey and Buck<sup>20]</sup>. We note that the experimental values in the minima at masses 55, 140 and 200 are lower than the predictions by almost an order of magnitude. This behaviour is theoretically not yet fully understood. But there is some indication from measurements in the 55-mass region, that the absorptive potential strength  $W$  is reduced near closed shell due to the smaller density of the final states<sup>20]</sup>.

Another investigation is connected with average neutron widths. Once such information is available, it is interesting to examine which portion of single particle strength is distributed over the analysed interval. In such studies the sums of the reduced widths for all s-, p- and d-wave neutron resonances can be compared with the Wigner limits for the reduced single particle widths. For the case of calcium the following results are obtained. For resonances in the excitation energies between 8.4 and 9.6 MeV 7.1% of the Wigner limit is observed for s-wave resonances, and 5.7% for d-wave resonances. Such fractions are reasonable for an interval of 1 MeV, since the average single particle width is typically spread over an interval of a few MeV. Only 1.1% of the total single particle strength for the odd parity p-wave resonances were seen. The latter fact seems to be consistent with the results from d,p measurements in calcium. These measurements below the neutron binding energy placed the unperturbed level positions of the p shell at 2.07 MeV and 4.13 MeV for  $2p_{3/2}$  and

$2p\ 1/2$ . Thus a very small fraction of the  $p$ -wave resonance strength should be observed in the neutron energy region of about 5 - 7 MeV higher in excitation energy.

### B. Investigation of Intermediate Structure

During the last decade a large number of neutron experiments have been performed, indicating that there is significant evidence for the phenomenological occurrence of intermediate structure in fast neutron interactions<sup>21]</sup>. Several examples have been given at this School. Such structure is characterized by widths ranging from  $\sim 50$  to several hundred keV. The theoretical basis for the understanding of intermediate structure phenomena has been given by Block and Feshbach in 1963.<sup>22]</sup> In their doorway state model these authors assumed that when a neutron enters an even-even nucleus it must lose first energy to one of the nucleons of the target before a complicated compound-nucleus state can be formed. The configuration resulting from the first collision should have two excited particles [ $2p$ ], including the incident neutron, and one hole [ $1h$ ] left by the nucleon struck. The two particle - one hole [ $2p-1h$ ] state is called a doorway between the single particle state in the entrance channel and the final many-nucleon excitation of the complex compound-nucleus state. If the  $2p-1h$  state has a reasonable lifetime, an intermediate resonance might be observed in the average cross section near the energy of the  $2p-1h$  state. Since all fine structure resonances contributing to the 'subgiant' or doorway structure are excited through the same nuclear state, namely the doorway resonance, the former resonances must all be of the same spin and parity. Applying, in addition, the intermediate coupling picture, the total reduced width of the doorway state is preserved in the sum of the corresponding reduced fine structure widths.

Most of the previous investigations in this field have been made by a simple search for significant structure of the predicted widths in the average excitation functions of total and partial cross sections. Although some results have been doubted, because of incorrect treatment of the data, there is serious evidence for the phenomenological appearance of intermediate structure from several independent<sup>1,21]</sup> investigations.

Unfortunately such results can not be used for an unambiguous identification of the nature of such structure. It has been shown that there is a rather high probability for spurious

intermediate structure, which can be caused by fluctuations in level widths and level spacings<sup>23]</sup>.

This difficulty has been mainly avoided in some more recent experiments in which intermediate structure phenomena were studied by angular and channel correlation measurements: Thus, for instance, some angular correlation measurements carried out at the Argonne National Laboratory<sup>21]</sup> have revealed significant correlated structure in some medium weight nuclei. In previous work at Karlsruhe<sup>24]</sup> it could be shown that intermediate structure is correlated in elastic and several inelastic channels of aluminum and iron. Although these experiments can probably be interpreted by means of the doorway picture, it is not fully satisfying from a theoretical point of view. An identification of a certain doorway state by direct rather than by indirect methods is much more desirable. As mentioned already, this can only be accomplished by showing that all fine structure resonances forming an intermediate resonance are all of the same spin and parity.

An experiment of this type has been made with the Karlsruhe cyclotron employing the 195 m flight path. An intermediate resonance in iron has already been suggested from a few previous experiments on total and differential elastic scattering<sup>56</sup> Fe. An experiment indicating this behaviour is shown in Fig. 14. Here we see the results obtained at Argonne National Laboratory from a transmission and an elastic scattering experiment in the energy range from 0.3 - 1.5 MeV<sup>25]</sup>. Especially in the experimentally averaged total elastic scattering cross sections in the top curve, we observe a broad structure near 770 keV. Shell model calculations, in addition, have indicated that there should be at least two  $2p-1h$  neutron states near the neutron binding energy having spin  $1/2^+$ . It has, therefore, been desirable for a long time to investigate  $s$ -waves resonances of this nucleus in the corresponding energy region. The result of a total neutron cross section measurement, recently carried out at Karlsruhe this region is shown in Fig. 15. This figure shows the transmission data for two largely different sample thicknesses in the range from 0.5 - 0.8 MeV. The solid lines represents an R-matrix multilevel least squares fit through both transmission curves simultaneously. It can be seen, that there are several broad  $s$ -wave dips centered around  $\sim 750$  keV.

If these  $s$ -wave resonances account for the observed intermediate resonance in the average cross section, a test of the sum rule for the reduced width must be positive. This possibility has been tested and the preliminary result is shown in Fig. 16. This diagram compares the summation of the reduced widths of  $s$ -wave resonances as a function of energy with the reduced

width of the intermediate resonance. Considering some uncertainties mainly due to the not yet investigated energy range above the inelastic threshold at  $\sim 850$  keV, Fig. 16 indicates remarkably good agreement with a sum rule. We might, therefore, tentatively consider this state to be a doorway resonance. For an unambiguous assignment it is necessary, in addition, to check whether the spacing and width distributions in this energy range deviates significantly from a statistical behaviour. Such tests including also information from measurements at other laboratories below 400 keV are presently underway but have not yet been completed.

#### V. Concluding Remark

The principle conclusion I would like to draw is that the modern high resolution neutron spectrometers have proven to be useful devices to furthering our understanding of neutron resonance reactions. In particular the isochronous cyclotron presently provides the high intensity necessary to perform high resolution differential resonance reaction measurements in the MeV range. This supposition forms the basis for systematic investigations of resolved resonances for higher partial waves. This is an important step, since most of our present knowledge on neutron resonances is due to experimental information below  $\sim 100$  keV, where s-wave scattering is predominant.

## References

1. J.A. Farrel, G.C. Kyker, E.G. Bilpuch, H.W. Newson, *Phys. Letters* 17 [1965] 286; C. Mahaux, *Proc. Int. Conf. on Nuclear Structure Studies with Neutrons*, Budapest, Hungary, 1972
2. J.A. Harvey, *Proc. Conf. on Pulsed High Intensity Neutron Sources*, 1966, USAEC CONF-650 271 p. 124; G.A. Bartholomew, P.R. Tuncliffe, *Intense Neutron Generator*, 1966, AECL-2600; A. Michaudon, *Seminar on Intense Neutron Sources*, Santa Fé, Sept. 1966, USAEC-CONF. 660 925, p. 789 ff; W.W. Havens, *ibid*, p. 565 ff
3. E. Rae, in *Experimental Neutron Resonance Spectroscopy*, ed. by J.A. Harvey, Academic Press, New York, 1970 p. 66 ff
4. J.A. Harvey, *Lecture, II. Int. School on Neutron Physics*, Alushta, USSR, April 2-19, 1974
5. S. Cierjacks, B. Duelli, P. Forti, D. Kopsch, L. Kropp, M. Lösel, J. Nebe, H. Schweickert, H. Unseld, *Rev. Sci. Instr.* 39 [1968] 1279; G. Schmalz, A. Schmidt, S. Cierjacks, H. Unseld, *A Coupled Electrostatic Deflector Assembly for Beam Deflection in an Isochronous Cyclotron*, to be published
6. G.J. Kirouac, J. Nebe, *Nucl. Phys.* A 154 [1970] 36; J. Nebe, *PhD Thesis*, University Karlsruhe, Febr. 1971
7. L. Kropp, P. Forti, *Nucl. Instr. Methods* 104 [1972] 381; L. Kropp, *PhD Thesis*, University Karlsruhe, Febr. 1971
8. S. Cierjacks, D. Kopsch, J. Nebe, G. Schmalz, F. Voß, *3rd Conf. on Neutron Cross Section and Technology*, Knoxville, USA, 1971, CONF-710 301, Vol. I, p. 280
9. F. Voß, S. Cierjacks, L. Kropp, *3rd Conf. on Neutron Cross Sections and Technology*, Knoxville, USA, 1971, CONF-710 301, Vol. I, p. 218; F. Voß, *PhD Thesis*, University Karlsruhe, 1972
10. A. Asami, M.C. Moxon, W.E. Stein, *Phys. Lett.* 28 B [1969] 656

11. G.J. Kirouac, J. Nebe, Report KFK 1069 [1969], J. Nebe, G.J. Kirouac, Report KFK 1189 [1970]; J. Nebe, G.J. Kirouac, Nucl. Phys. A 185 [1972] 113
12. E.P. Wigner, L. Eisenbud, Phys. Rev. 72 [1947] 29
13. J.M. Blatt, L.C. Biedenharn, Rev. Mod. Phys. 24 [1952] 258
14. G. Racah, Phys. Rev. 61 [1942] 186, 62 [1942] 438
15. R. Huby, Proc. Phys. Soc. 67A [1954] 1103
16. A. Gilbert, A.G.W. Cameron, Can. J. Phys. 43 [1965] 1446
17. E. Bilpuch, Proc. Int. Conf. on Statistical Properties of Nuclei, Albany, Aug. 1971
18. S. Cierjacks, R.R. Spencer, unpublished
19. V.G. Soloviev, Ch. Stoyanov, A.I. Vdovin, Nucl. Phys. to be published
20. C.M. Newstead, J.P. Delaroche, B. Cauvin, Conf. on Nucl. Structure Studies with Neutrons, Budapest, p. 144, F. Perey, B. Buck, Nucl. Phys. 32 [1962] 353
21. J. Cabe, Report CEA-3279, 1967; A.J. Elvin, J.E. Monahan, Nucl. Phys. A 123 [1969] 33; A.B. Smith, J.F. Whalen, K. Takeuchi, Report ANL-7564 [1969]
22. B. Block, H. Feshbach, Ann. Phys. 23 [1963] 47, H. Feshbach, Conf. on Direct Interactions and Reactions Mechanisms, Padua, Italy, 1962 and Int. Conf. on the Study of Nuclear Structure with Neutrons, Antwerp, 1965, North Holland Press, 1966, p. 257
23. P.P. Singh, Hoffmann-Pruther, D.W. Lang, Phys. Lett. 23 [1966] 255
24. F. Voß, S. Cierjacks, Int. Conf. on Nucl. Structure Studies with Neutrons, Budapest, Hungary, 1972, p. E 13
25. A.B. Smith, D. Lister, IAEA Conf. on Nucl. Data Microscopic Cross Sections and Other Data Basic for Reactors, Paris, 1966, P. CN-23/49

Table 1: Spacing of resonances in  $^{41}\text{Ca}$  above the neutron binding energy

Number of resonances	l	J	$\bar{D}_{lJ}^{\text{exp}}$ [keV]	$\bar{D}_{lJ}^{\text{corr}}$ [keV]
28	0	1/2	$45^{+4}_{-6}$	45
12	1	1/2	$55^{+10}_{-24}$	
13	1	3/2	$54^{+10}_{-17}$	
25	1		$28^{+5}_{-12}$	22
12	2	3/2	$61^{+16}_{-32}$	
9	2	5/2	$82^{+16}_{-42}$	
21	2		$35^{+10}_{-17}$	12

Table 2 : Neutron strength functions  $S_{lJ}$  for s-, p- and d-wave resonances in  $^{40}\text{Ca}[n, n]$

Number of resonances	l	J	$\bar{\Gamma}_n^o$ [keV]	$S_{lJ} \times 10^4$
28	0	1/2	13.2	$2.92^{+1.25}_{-0.57}$
12	1	1/2	2.66	$0.47^{+0.38}_{-0.14}$
12	1	3/2	1.64	$0.29^{+0.23}_{-0.09}$
24	1		2.15	$0.35^{+0.15}_{-0.08}$
10	2	3/2	22.0	$3.4^{+3.2}_{-1.1}$
9	2	5/2	7.8	$0.9^{+0.9}_{-0.3}$
19	2		15.3	$1.9^{+1.0}_{-0.5}$

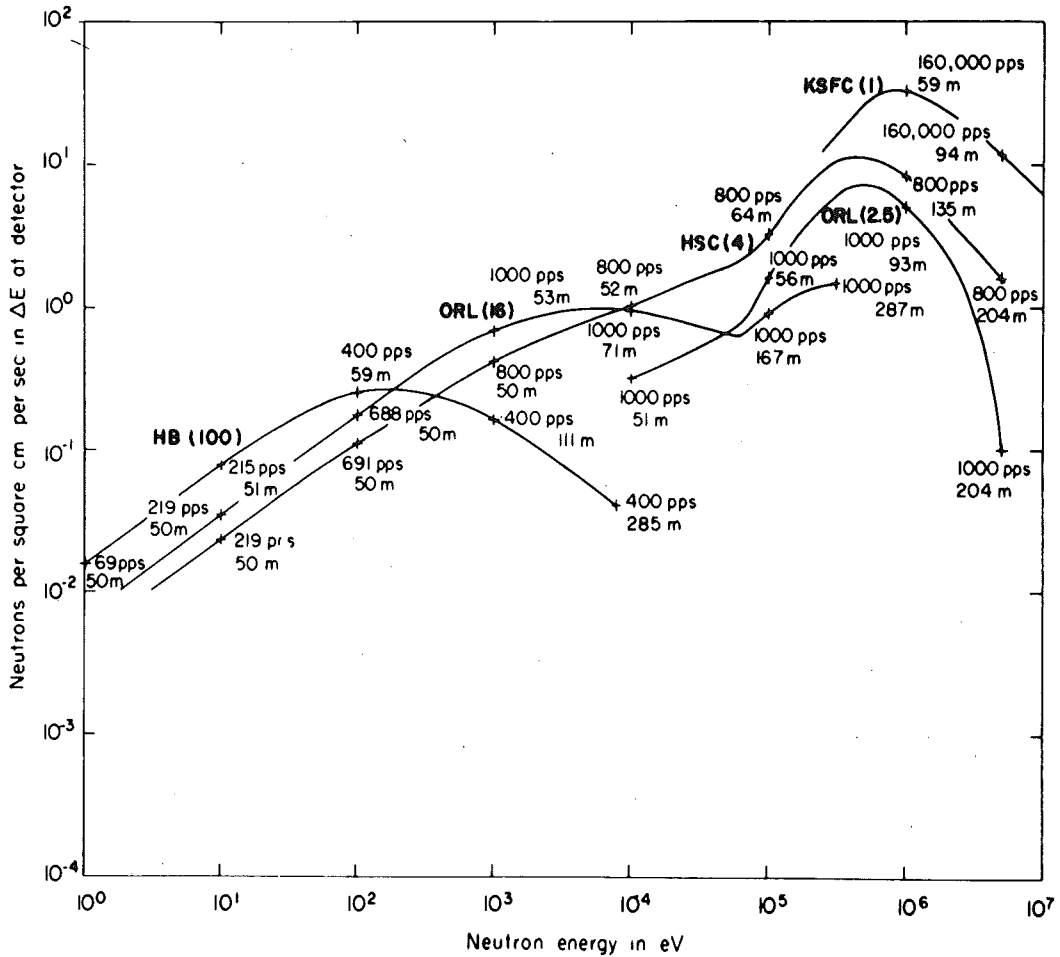


Fig. 1: Comparison of advanced high resolution neutron spectrometers. The quality of a neutron spectrometer is measured in terms of the useful flux available at the detector for an effective energy resolution of  $\Delta E/E = 8.8 \times 10^{-4}$  [comp. ref. 3]

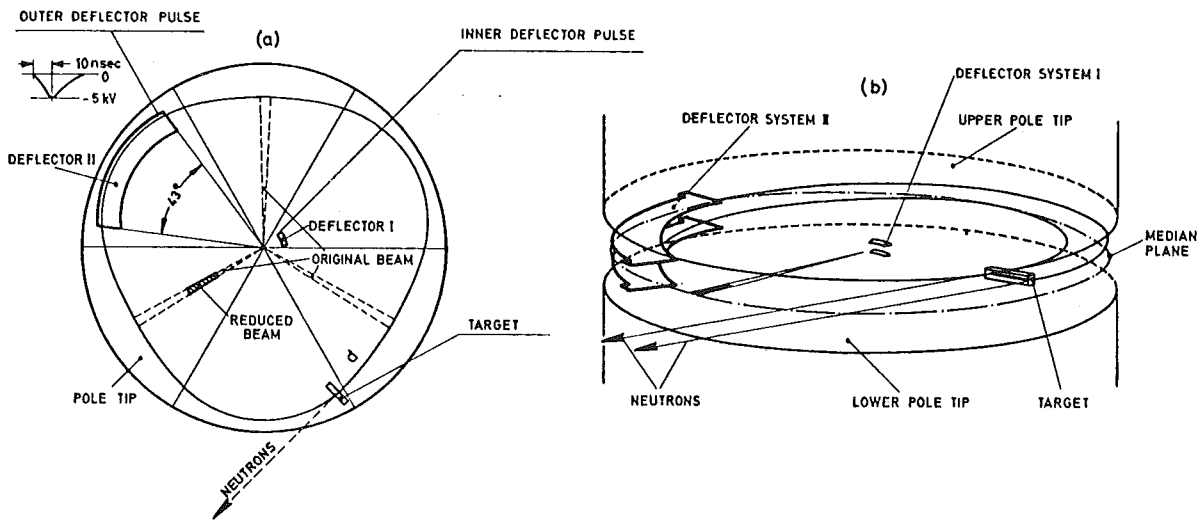


Fig. 2: Principle of the deflection bunching system  
 a) Top view of the cyclotron chamber showing the position of the deflectors  
 b) Schematic drawing illustrating the deflection of ion packets onto the neutron producing target

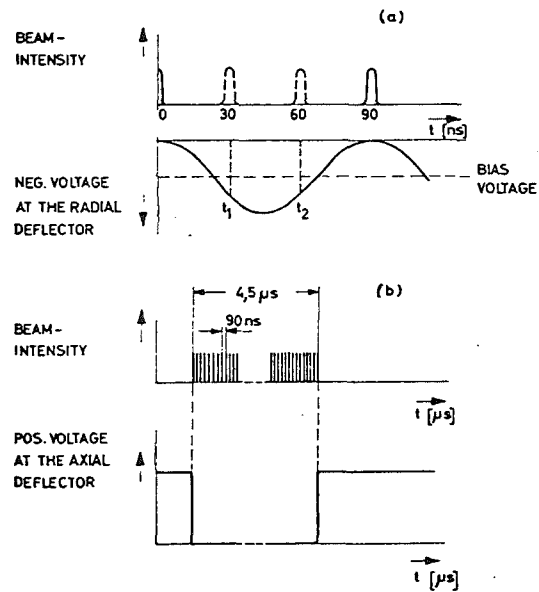


Fig. 3: Voltages applied to the inner deflector assembly illustrating the principle of beam suppression

- a] Elimination of 'two out of three' micro-structure pulses with a radial deflector
- b] Formation of  $4.5 \mu$ sec ion packets with an axial deflector of system I

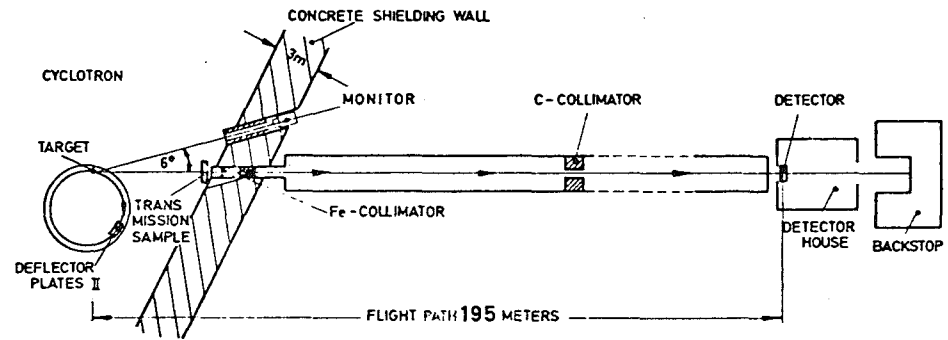


Fig. 4: Top view of the Karlsruhe neutrom time-of-flight spectrometer

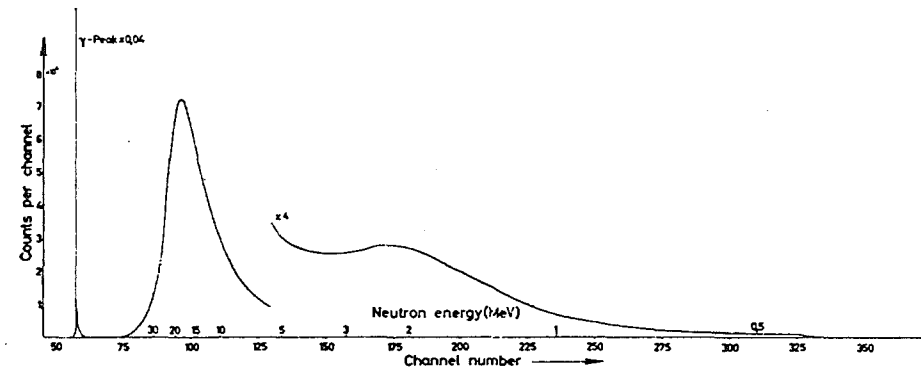


Fig. 5: Typical unmoderated neutron time-of-flight spectrum obtained from bombardment of a natural uranium target with 50 MeV deuterons

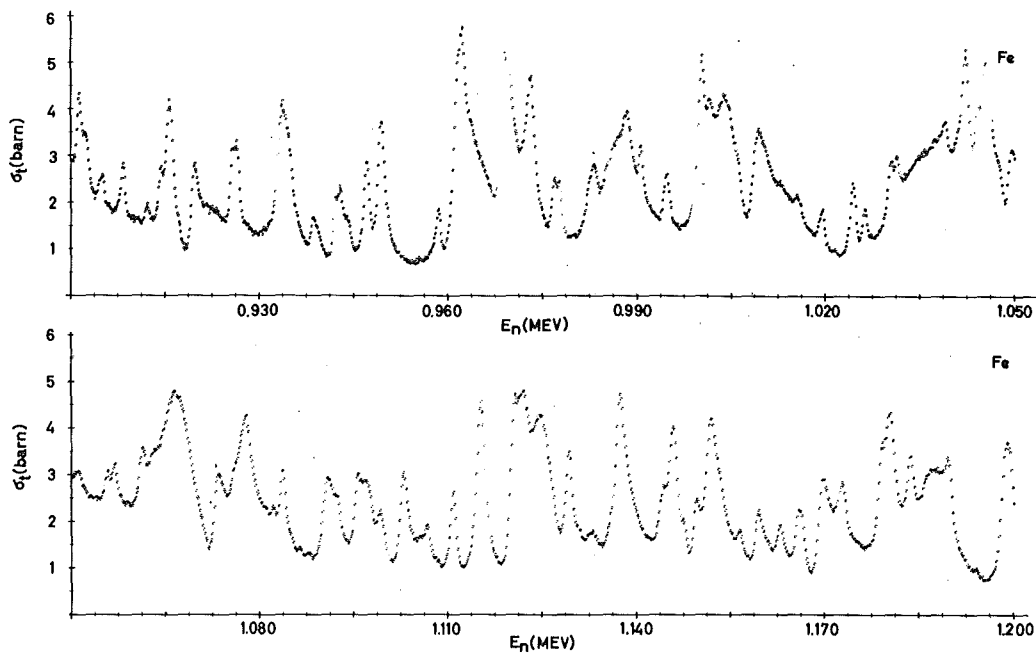
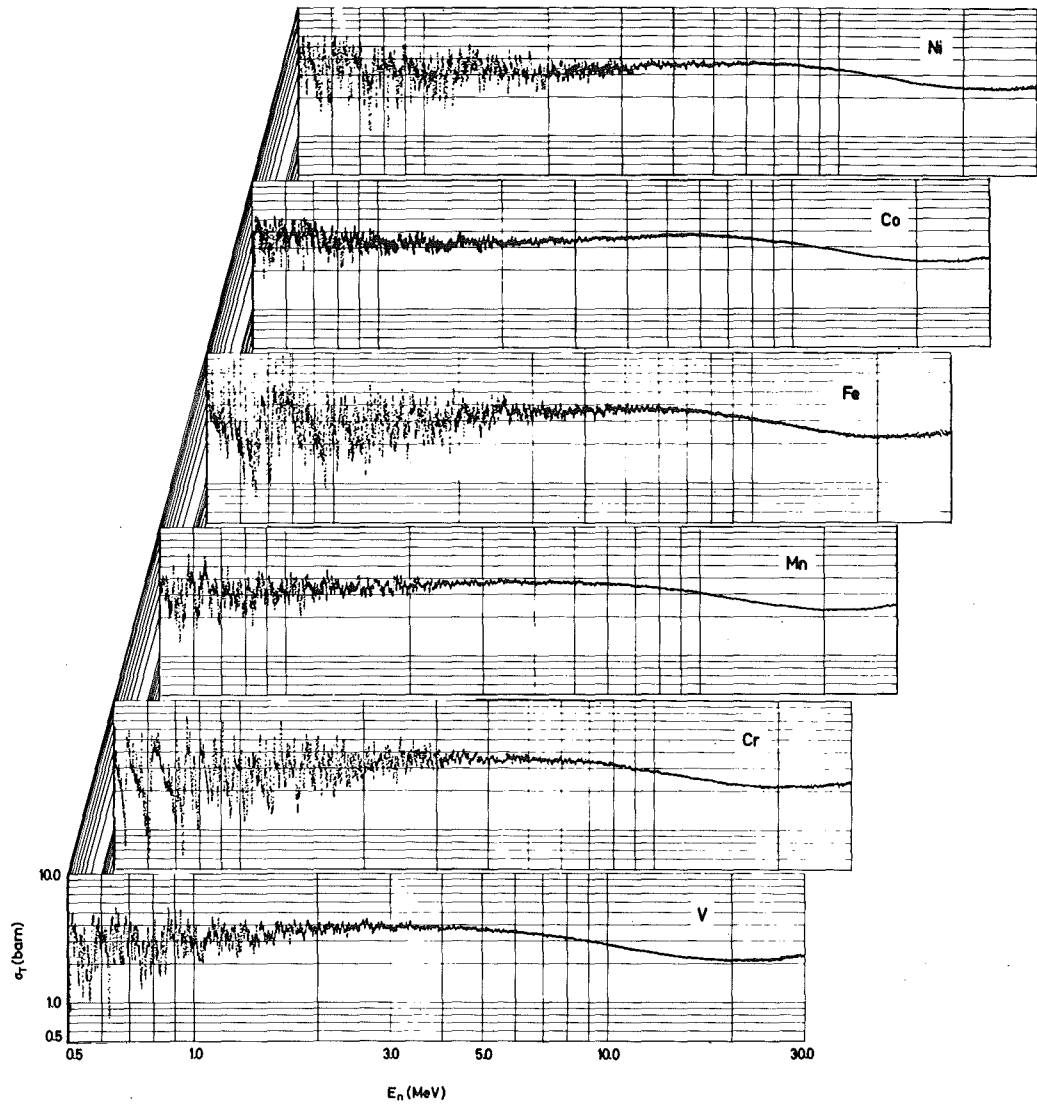


Fig. 6: a] Total neutron cross sections of some medium weight nuclei  
b] Partial results of the total neutron cross section of iron between 0.9 - 1.2 MeV

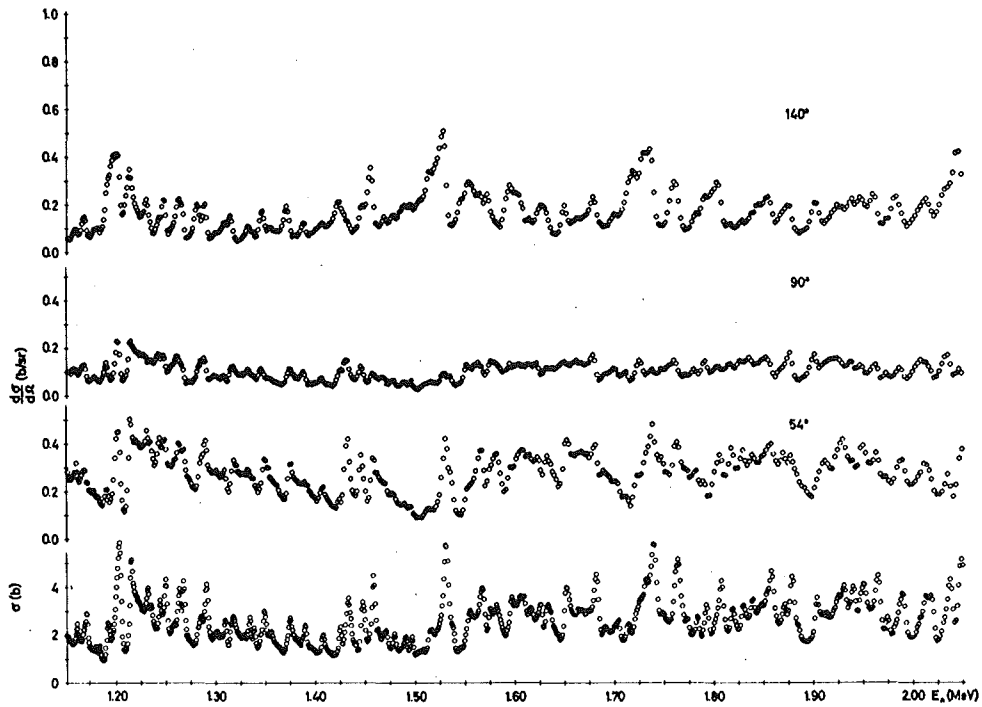


Fig. 7: Total and differential neutron cross sections for  $^{40}\text{Ca}$  between 1.2 - 2.0 MeV

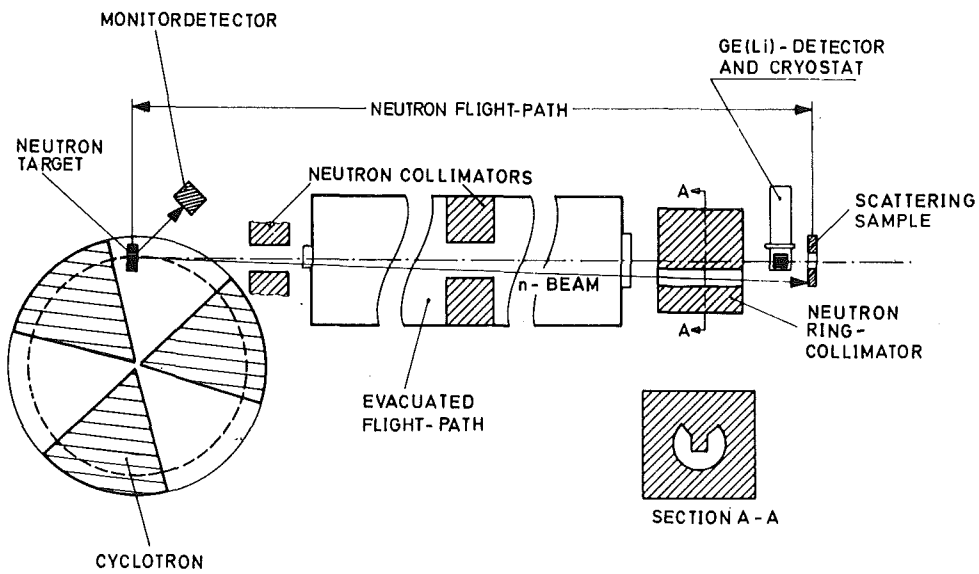


Fig. 8: Scheme of the Karlsruhe experimental device used for the investigation of neutron inelastic scattering

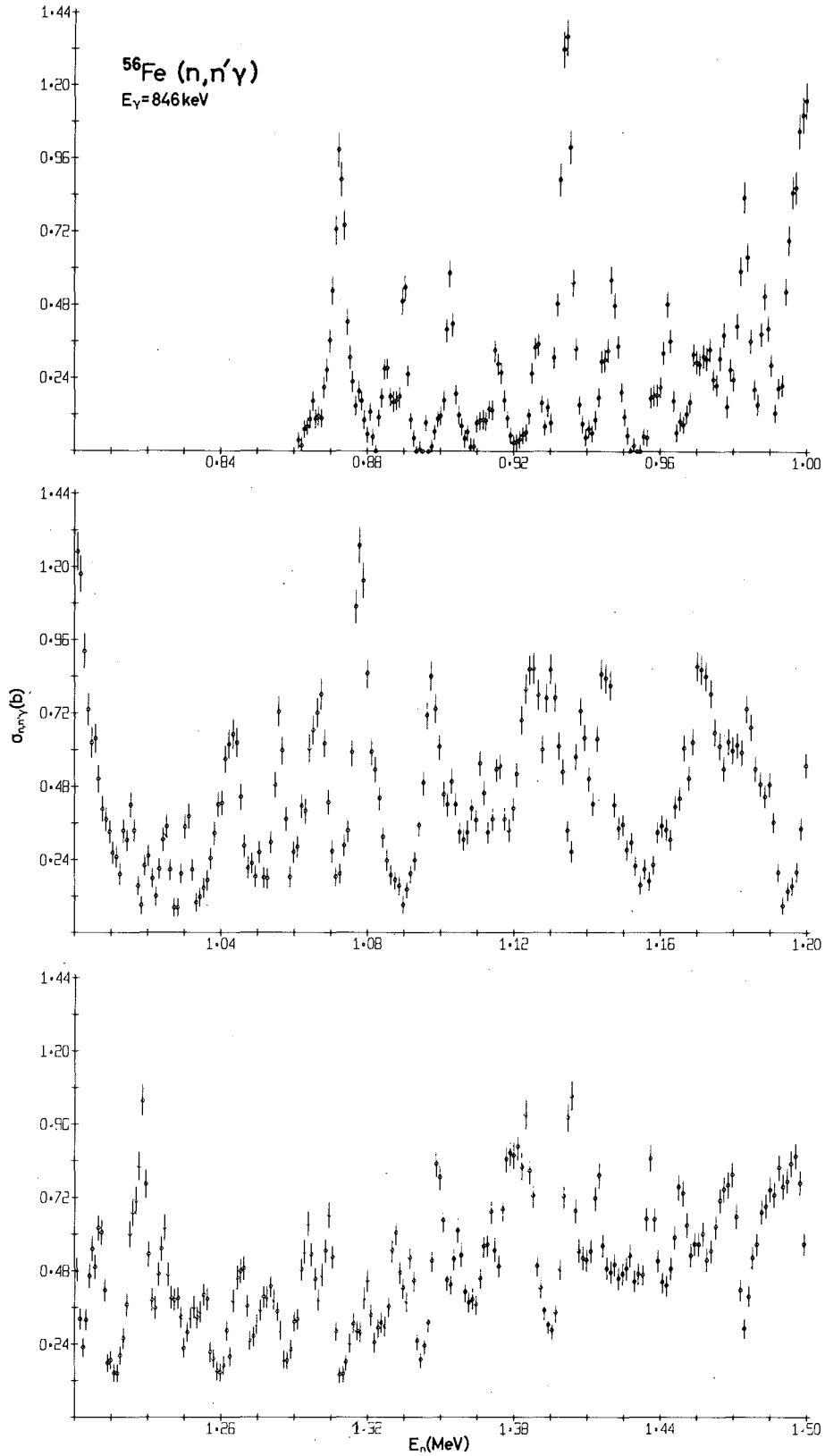


Fig. 9: Cross section for the inelastic scattering to the 846 keV level in  $^{56}\text{Fe}$  between 0.8 - 1.5 MeV

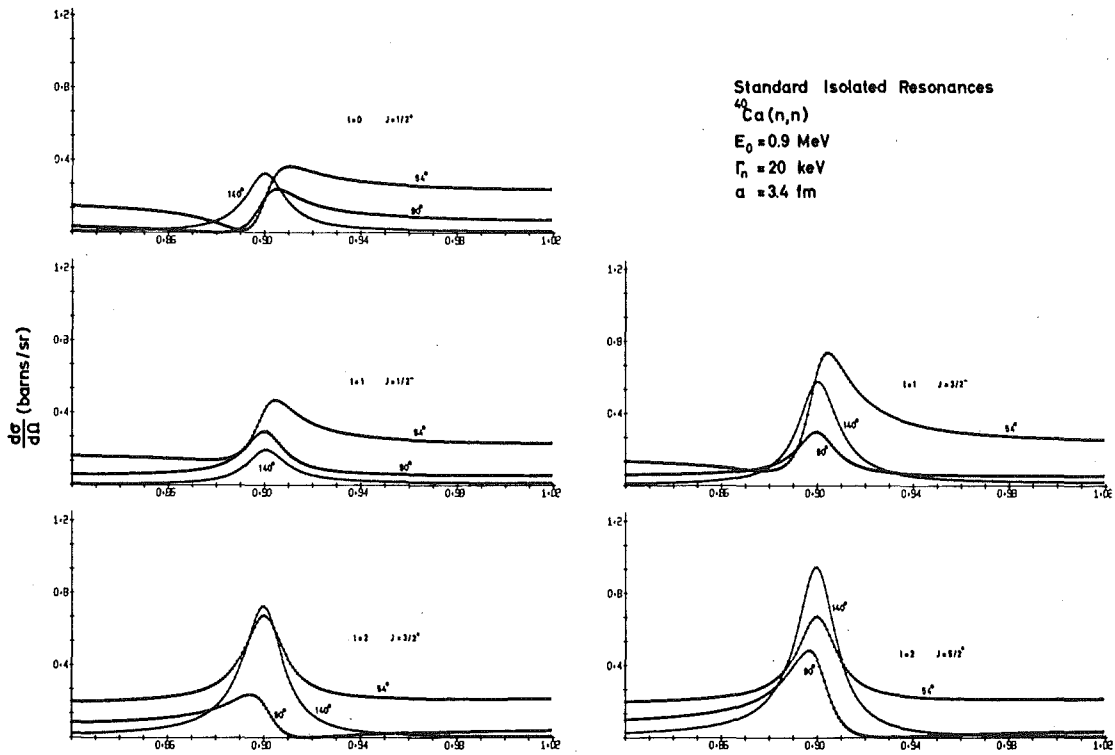


Fig. 10: Examples of isolated s-, p- and d-wave standard resonances for  $^{40}\text{Ca}$  [n, n]

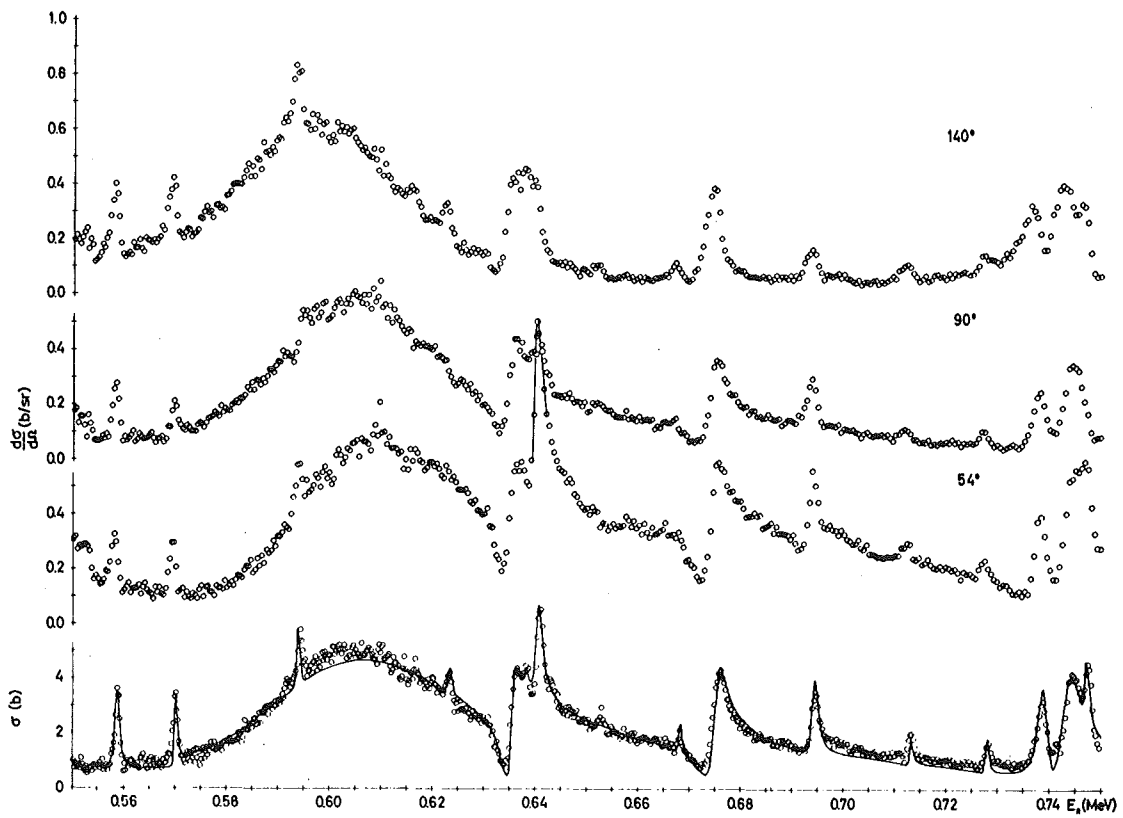


Fig. 11: Total and differential elastic scattering cross sections for  $^{40}\text{Ca}$ . The solid line in the bottom curve results from an R-matrix calculation using the spin assignments obtained from the differential data

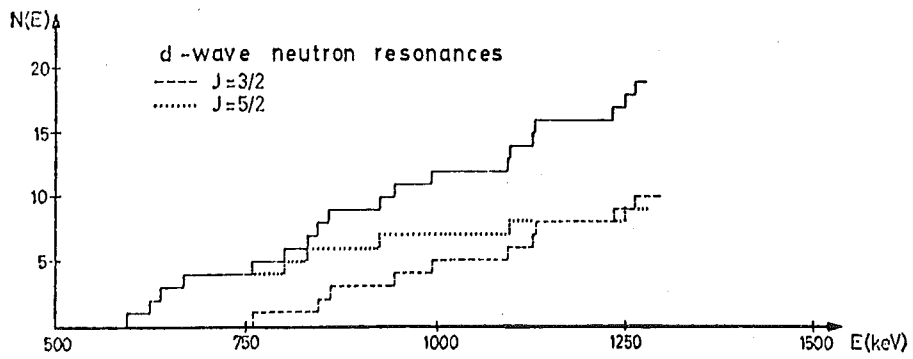
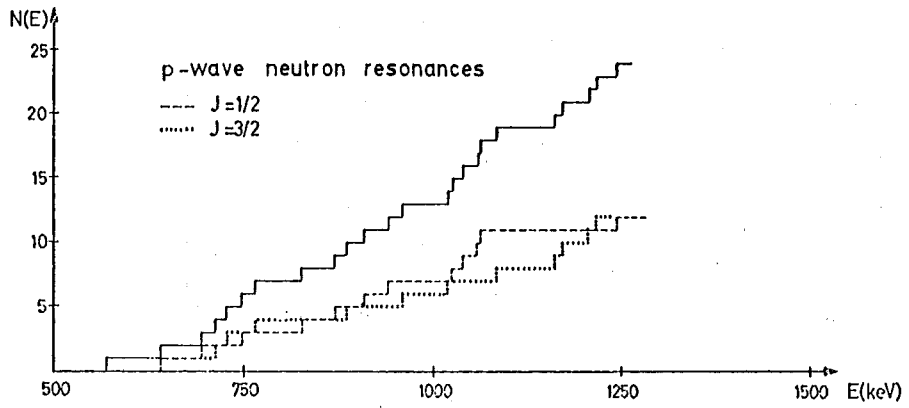
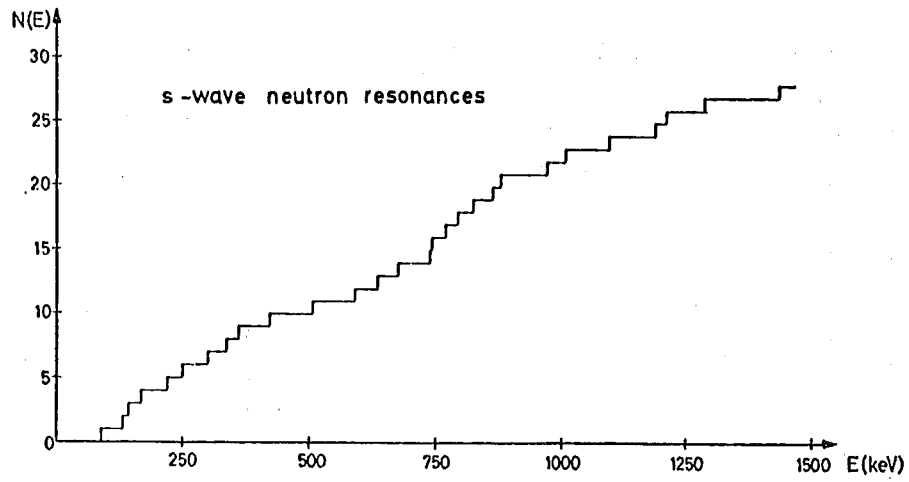


Fig. 12: Level spacings of s-, p- and d-waves resonances observed in the  $^{40}\text{Ca} [n, n]$  reaction

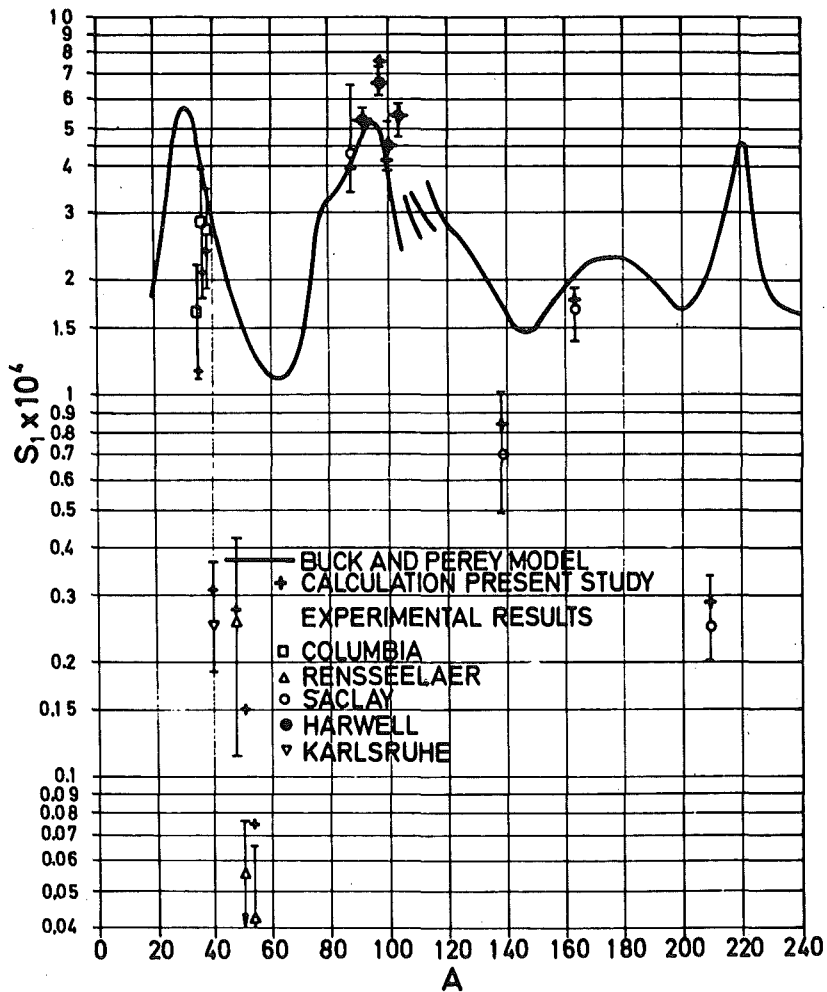


Fig. 13: Selected experimental and theoretical results for the p-wave strength function

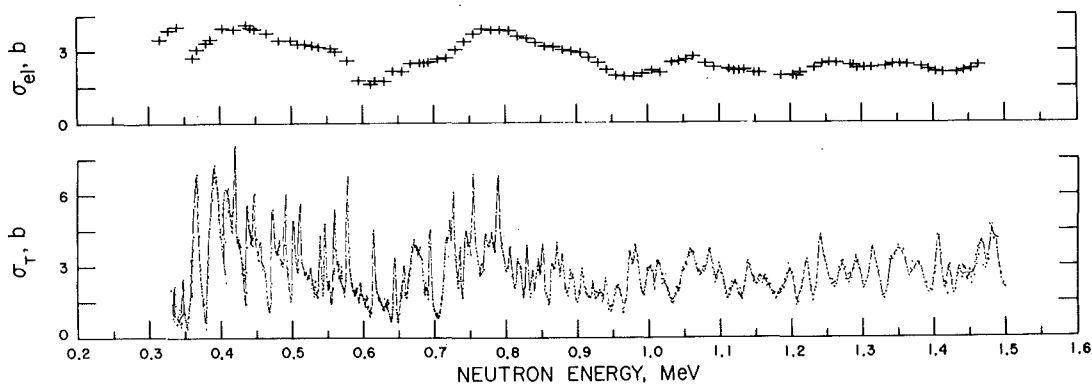


Fig. 14: High resolution total cross section and 50 keV average of measured elastic scattering cross section of Fe. [taken from ref. 25]

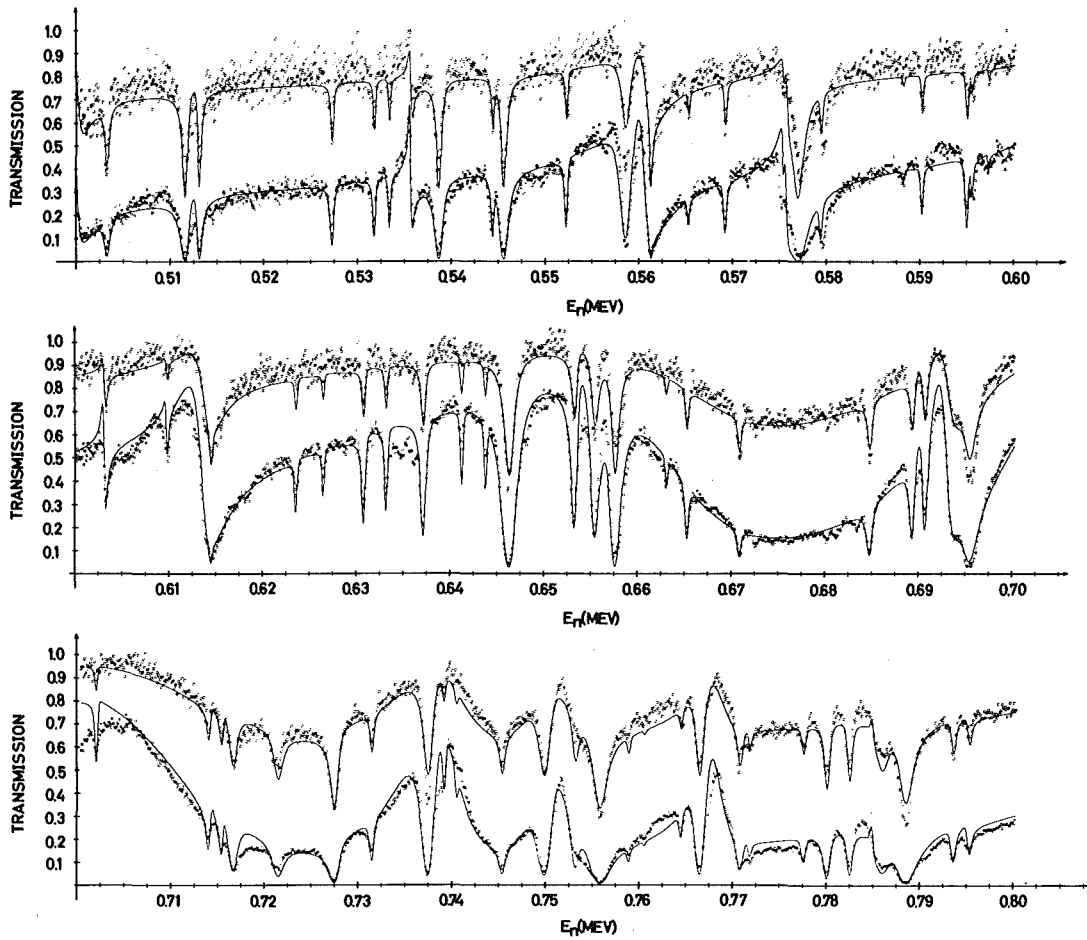


Fig. 15: Transmission data of Fe taken for two different sample thicknesses. The solid curve represents a multilevel least squares fit to both transmission curves simultaneously

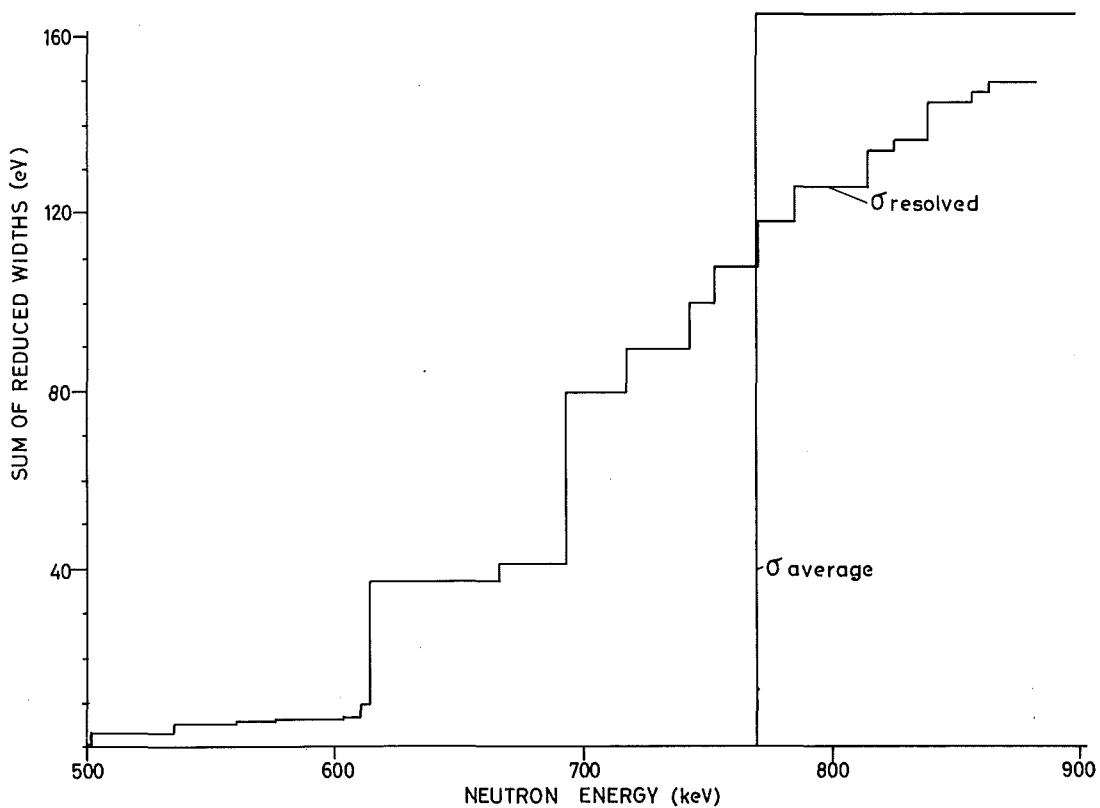


Fig. 16: Check of the sum rule for s-wave fine structure resonances forming the intermediate resonance in the average total cross section of iron near 770 keV [preliminary]